Au-Mediated Growth of Wurtzite ZnS Nanobelts, Nanosheets, and Nanorods via Thermal Evaporation

Changhao Liang,[†] Yoshiki Shimizu,[†] Takeshi Sasaki,[†] Hiroyuki Umehara,[‡] and Naoto Koshizaki*,[†]

Nanoarchitectonics Research Center (NARC), National Institute of Advanced Industrial Science and Technology (AIST), Central 5, 1-1-1 Higashi, Tsukuba, Ibaraki 305-8565, Japan, and Metrology Institute of Japan (MIJ), National Institute of Advanced Industrial Science and Technology (AIST), Central 5, 1-1-1 Higashi, Tsukuba, Ibaraki 305-8565, Japan

Received: December 22, 2003; In Final Form: April 7, 2004

In this study, we demonstrate the large-scale synthesis of wurtzite ZnS nanostructures by simple thermal evaporation of ZnS powder in the presence of Au catalysts at 970 °C. Scanning electron microscopy (SEM), transmission electron microscopy (TEM), and X-ray diffraction (XRD) analyses demonstrated that the ZnS nanostructures consisted of nanobelts, nanosheets, and nanorods with a hexagonal wurtzite structure. The nanobelts have lengths ranging from tens to hundreds of micrometers, thicknesses of tens of nanometers, and widths ranging from hundreds of nanometers to the order of micrometers. The preferred growth axis of single crystalline nanobelts was found to be [01-11] or [0001]. Large single crystalline nanosheets also formed with flat surfaces. ZnS nanorods grew preferably in the [0001] direction with uniform diameters, with their ends attached to Au particles. Small amounts of bicrystal and tricrystal nanobelts were also observed. The formation of ZnS nanostructures with various morphologies was mainly due to the local concentration difference of ZnS vapor. The growth process was proposed on the basis of vapor−liquid−solid (VLS) and/or vapor−solid (VS) crystal growth mechanisms. Room-temperature photoluminescence measurements showed that the synthesized ZnS nanostructures had a strong green emission band at a wavelength of 522.5 nm, which may be ascribed to deep-level emissions induced by defects and/or Au impurity.

1. Introduction

The synthesis of single crystalline semiconducting nanostructures such as nanowires and nanobelts/ribbons has attracted great interest due to their sizes, morphology-related properties, and their emerging applications in functional nanodevices, such as nanowire-based nanolasers,[1] nanobelt/ribbon-based nanosensors,[2] field-effect transistors,[3] and nanocantilevers.[4] ZnS is a wide band gap II−VI ($E_g \approx 3.7$ eV at 300 K) semiconducting material, and is used commercially as a phosphor and in thin-film electroluminescent devices.[5] ZnS crystals doped with transition-metal or rare-earth metal ions can exhibit a variety of luminescent properties, such as photoluminescence,[6] electroluminescence,[7] thermoluminescence,[8] and triboluminescence.[9] One-dimensional single crystalline ZnS nanostructures may also lead to novel properties that can be applied to the development of new nanostructure-based devices. Recently, synthesis and characterization of ZnS nanowires and nanobelts has been the focus of increasing research interest. ZnS nanowires can be synthesized using a liquid crystal template,[10] a micelle template,[11] or by thermal evaporation at 900 °C using Au as a catalyst.[12] In contrast, the synthesis of ZnS nanobelts has only been achieved by simple thermal evaporation of ZnS powders, in the presence of Au catalysts at 1200 °C,[13] using rf inductive heating in an atmosphere consisting of CO and H_2,[14] by hydrogen-assisted synthesis at 1100 °C,[15] or at 1050 °C together with the formation of ZnS combs and windmill-like structures.[16] Thus, using the thermal evaporation method, ZnS nanowires can be produced at relatively low temperatures by catalyst-assisted vapor−liquid−solid (VLS) growth, whereas nanobelts/ribbons have only been produced at temperature higher than the phase transformation temperature (∼1020 °C[17]) of ZnS from cubic to hexagonal (wurtzite-2H) structure, and the growth process is mainly explained on the basis of the vapor−solid (VS) process as has been reported for oxide nanobelt/ribbon growth.[18] In this paper, we report the large-scale synthesis of wurtzite ZnS nanobelts by simple thermal evaporation of ZnS powder at a relatively lower temperature of 970 °C in the presence of Au catalysts. Characterization, growth process, and photoluminescence properties of the ZnS nanostructures are also reported.

2. Experimental Section

A high-temperature horizontal tube furnace (SiC heater) was used to synthesize the ZnS nanostructures. An alumina tube with an outer diameter of 42 mm, inner diameter of 35 mm, and length of 700 mm was installed in the furnace. Another ceramic tube with an outer diameter of 30 mm, inner diameter of 24 mm, and length of 500 mm was inserted into the alumina tube. Zinc sulfide powder (99.99% pure) was loaded into a ceramic boat that was positioned inside the ceramic tube and placed in the center of the furnace. A piece of sapphire (0001) substrate (6 mm × 8 mm in size) coated with Au film (about 70 nm thick) was placed against the inner wall of the second ceramic boat that was inserted into the thinner ceramic tube on the downstream side. The substrate was approximately 5 cm from

* Author to whom correspondence should be addressed. Fax: +81-298-61-6355. E-mail: koshizaki.naoto@aist.go.jp.
[†] Nanoarchitectonics Research Center.
[‡] Metrology Institute of Japan.

10.1021/jp037963f CCC: $27.50
Published on Web 06/09/2004

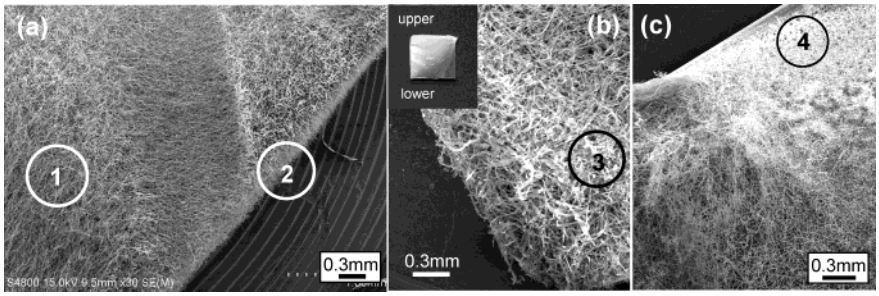

Figure 1. (a), (b), (c) Low-magnification SEM images of ZnS nanostructures synthesized via simple thermal evaporation of ZnS powder at 970 °C. The inset in (b) represents an optical image of the entire substrate covered with product. (a), (b) and (c) are taken from the middle left edge, the upper left corner, and the middle right edge of the substrate in the optical image. The upper left corner is the part closest to the ZnS vapor source.

the center of the source powder. After the system was evacuated to a base pressure of 5×10^{-2} Torr, high-purity Ar carrier gas was added at a flow rate of 120 sccm (standard cubic centimeters/minute). The furnace was heated to 970 °C over a 10 min period, and maintained at that temperature for 2 h under a pressure of 350 to 400 Torr. The temperature of the substrate area was 750 to 800 °C. The furnace was then cooled to room temperature and the gas supply was disconnected. The temperature and reaction time of the furnace were program-controlled.

A white wool-like product was observed on the surface of the sapphire substrate. This product was characterized by X-ray diffraction (XRD, Rigaku RAD-C, 1.54056 Å Cu Kα radiation, scanning rate of 0.5°/min), and a field-emission scanning electron microscopy (FE-SEM, Hitachi S-4800). The product was scraped off the substrate and suspended in ethanol solution. The suspension was then ultrasonicated and deposited onto a holey carbon-coated copper grid for transmission electron microscopic (TEM, JEOL JEM-2000FXII at 200 kV, JEOL JEM-2010 at 200 kV) observation and energy-dispersive X-ray spectroscopic (EDS, EDAX DX-4) analysis. The photoluminescence (PL) spectrum was measured at room temperature using a He−Cd laser as an excitation source with a wavelength of 325 nm.

3. Results and Discussion

Figure 1 (a, b, c) shows the overall morphology of the product that was deposited on the sapphire substrate. The density of the deposits gradually decreased from the upper to the lower part of the substrate from the optical image (see inset of Figure 1b). A large quantity of belt-like or sheet-like structures was observed from different areas of substrate. Close examination of the product revealed the formation of several types of structures. Figure 2 depicts the high-magnification SEM images taken from the circled areas (1 to 4) in Figure 1. The most commonly observed structures were ultra-long nanobelts (from tens to hundreds of micrometers in length) with some aligned growth (Figure 2a, from area 1), having widths ranging from hundreds of nanometers to several micrometers and thicknesses about tens of nanometers. The edges of the nanobelts were either smooth or saw-like (Figure 2c). The shape at the top of the belt could clearly be observed from the view taken at the substrate edge (Figure 2b, from area 2). The width of the belts gradually decreased, ending with pseudo-rectangular cross-sections or needle-like tips (Figure 2d). In addition, some particles were attached to the tips and the side edges of the belts (Figure 2e). This observation contrasts with what normally occurs with traditional VLS growth where in most cases catalyst particles are found at the tip end. Moreover, a few flag-like nanostructures were also observed (Figure 2f). The growth of the structures initiated from stable rod formation, with some larger triangle-shaped sheets protruding epitaxially from the side face. Figure 2g (from area 3) shows many large sheet-like structures grown near the upper edge of the substrate. The widths of these sheets exceeded those of the belts although they were shorter in length. It was also observed that the lower area of the substrate was sparsely covered with straight belts and rod-like structures (Figure 2h from area 4). Numerous round particles with bright contrast were attached to the end of the structures or were protruding from the large ZnS crystals on the substrate. Observation of the root part of the belts or rods indicated that the structure formation was initiated by nucleation at the side facets of the ZnS crystal (see inset of Figure 2h). It is likely that a coherent epitaxial relationship may exist between the nanostructures and the aggregated ZnS crystals.

The phase structure and purity of the synthesized product was analyzed by X-ray diffraction. Figure 3a shows the XRD spectrum obtained from the deposited materials together with the sapphire substrate. The *c*-plane diffraction of the sapphire substrate was not detected. This might have been caused by an inappropriate angle of the substrate surface with respect to the X-ray beam. All of the peaks were well indexed according to the three phases as shown in spectrum. (1) Wurtzite-2H (hexagonal) ZnS with lattice constants of $a = 3.821$ Å and $c = 6.258$ Å was in good agreement with the reported values ($a = 3.8209$ Å, $c = 6.2573$ Å) from JCPDS, No. 36-1450 within the range of experimental error. Wurtzite-2H ZnS formed during the rapid thermal evaporation process at 970 °C, although the bulk cubic ZnS is known to transform into wurtzite-2H ZnS at temperatures higher than 1020 °C.[17] (2) Face-centered cubic Au with a strong (111) peak at 38.20° of 2θ (JCPDS, No. 04-0784). 3) Sphalerite (cubic) ZnS structure ($a = 5.406$ Å, JCPDS, No. 05-0566). One broad peak and one sharp peak overlapped at a position of 69.28° (2θ scale). This was indexed to the (400) plane. The nanostructures that formed by thermal evaporation were clearly in wurtzite-2H ZnS structure. The Au phase came mainly from aggregated particles from Au-coated film. The cubic ZnS may have resulted from ZnS particles condensed directly from the ZnS vapor. For further confirmation, a part of the wool-like material was scraped from the sapphire substrate and suspended in ethanol solution. Several drops of the suspension were then deposited on a quartz substrate for XRD analysis. Only diffraction peaks from wurtzite-2H ZnS were detected (Figure 3b).

The structure, morphology, and composition of a single ZnS nanostructure were further characterized using TEM, FE-SEM, and EDS. Figure 4a shows the typical TEM image of the ZnS nanobelts as depicted in Figure 2a with smooth surfaces and uniform widths. The ripple-like contrast of the belts in the TEM

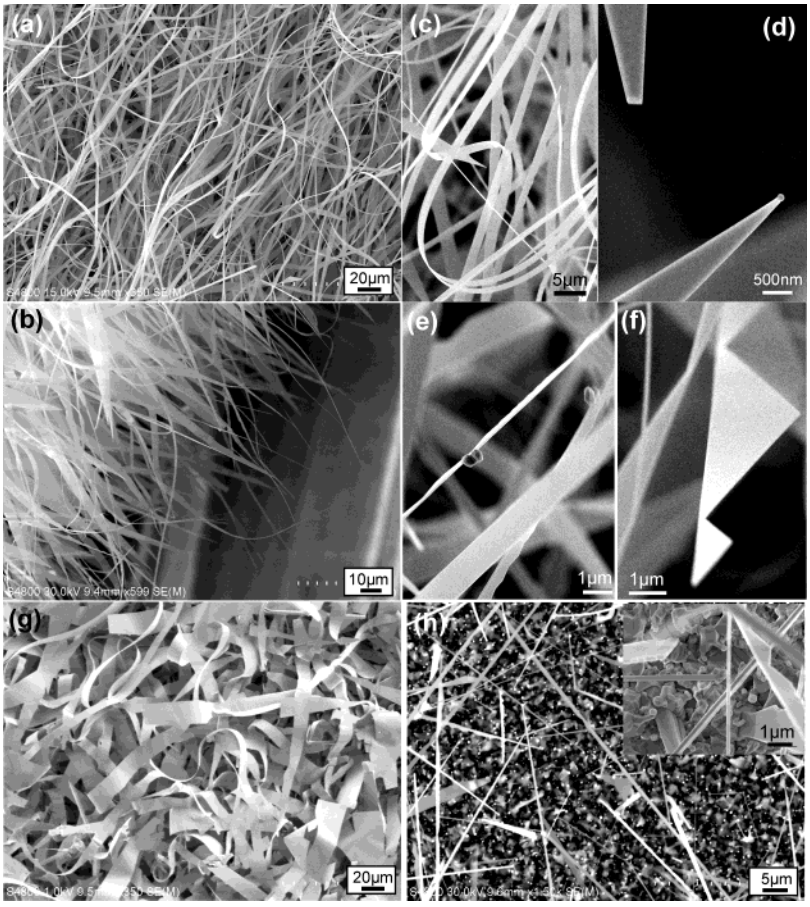

Figure 2. (a)−(h) FE-SEM images showing the typical morphology of the as-synthesized ZnS nanobelts, nanosheets, and nanorods from different areas of the substrate as circled in Figure 1. (a), (c) are from area 1; (b), (d)−(f) are from area 2; (g) is from area 3; and (h) is from area 4. The inset in (h) shows the root part of the nanobelts and nanorods grown from ZnS crystals.

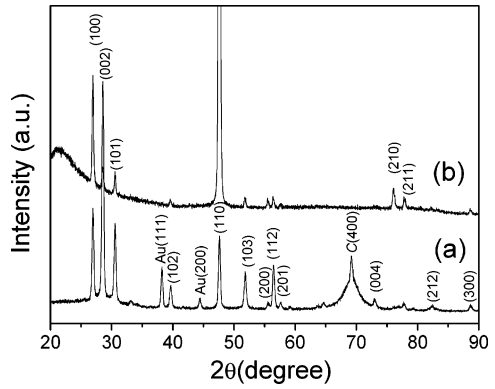

Figure 3. (a) XRD pattern of synthesized products on the substrate. Three phases, ZnS in wurtzite structure, ZnS in sphalerite structure (marked as *c*), and fcc Au phase, were indexed. (b) XRD pattern of belt-like or wire-like product scraped from the substrate. Only the wurtzite ZnS structure was revealed.

image was due to the bend contours, as typically observed in the TEM observation of slightly bent thin crystals.[19] Bicrystal-like belts were also observed in the product (Figure 4b). These structures were similar to those recently synthesized via thermal evaporation of a powder mixture of ZnS and SiO.[20] The transmission electron diffraction (TED) pattern obtained from the boundary area between the two belts presented two sets of similar patterns that could be indexed along the [2-1-10] zone axis, as shown in Figure 4c. FE-SEM observation of the sample on the TEM grid (Figure 4d) revealed that the bicrystal was constructed from two belts connected along one axis in a "V" shape. Another rod-like structure (indicated by an arrow in Figure 4a) was found with dark contrast on the surface of one of the belts. FE-SEM images (Figures 4e and 4f) showed that this structure was a tricrystal consisting of three thin belts either in a "Y" shape connected along one axis (the inset of Figure 4e) or a "Z" shape connected along two axes (the inset of Figure 4f).

Figure 5a shows a typical TED pattern recorded for a single crystalline belt, which could be indexed to diffraction reflections along the [2-1-10] zone axis of the single crystal with a hexagonal structure. The corresponding HRTEM (Figure 5b) image also indicated perfect wurtzite-2H structures. The measured lattice spacing of 6.26 Å corresponded to the (0001) plane. The angle measured between the [0001] direction and the preferred growth axis [01-11] of this belt was found to be approximately 62°, which is in good agreement with the calculated angle between (0001) and (01-11) planes of 62.12° (Figure 5c). In addition, we also detected some belts with [0001] preferred growth axis, and some belts with stacking faults. Figure 5d presents the corresponding HRTEM images of one bicrystal belt as displayed in Figure 4b. The angle between the (0002) planes in the two nanobelts was 116° (as indicated in Figure 5d). The preferred growth axis of the bicrystal belts was thus estimated to be [01-13] (Figures 5d and 5e). An amorphous feature existed along the high-angle grain boundary. Figure 6a presents a saw-like nanobelt with regular notches along one of the edges. Figure 6b presents a single crystalline nanosheet with the shape of a parallelogram with supplementary angles of 80° and 100°. The TED pattern recorded along the [2-1-10] zone axis without any tilt was similar to that of the belts. The side

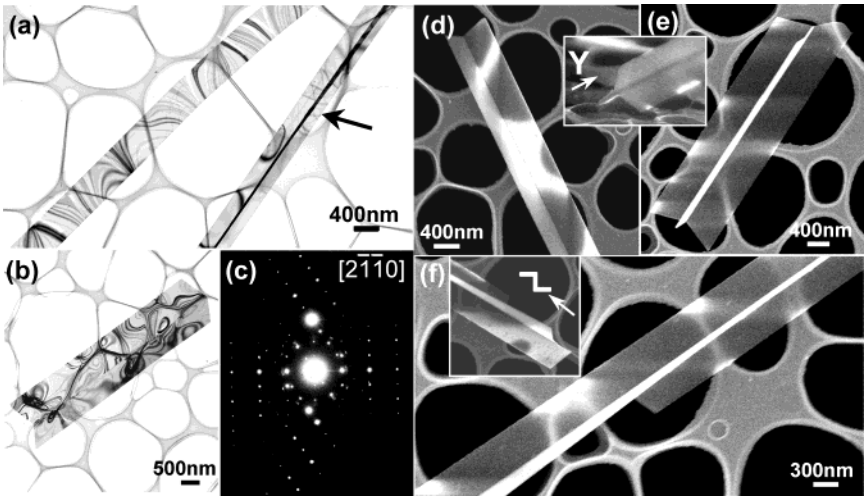

Figure 4. (a)−(f) TEM images, TED patterns, and FE-SEM images of single ZnS nanobelts. Bicrystal and tricrystal nanobelts are shown.

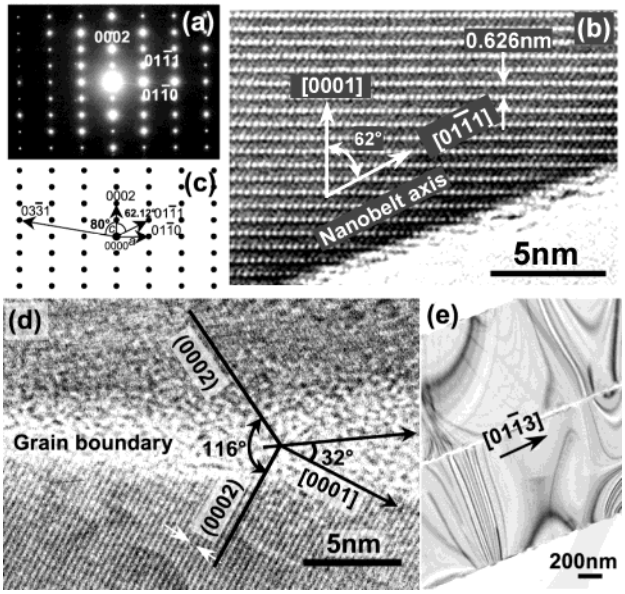

Figure 5. (a) TED pattern and (b) HRTEM image of single crystalline ZnS nanobelts. (c) Schematic illustration of TED spots and growth orientation of ZnS nanobelts and nanosheets (as shown in Figure 6(b)). (d) HRTEM image and (e) TEM image of one bicrystal ZnS nanobelt.

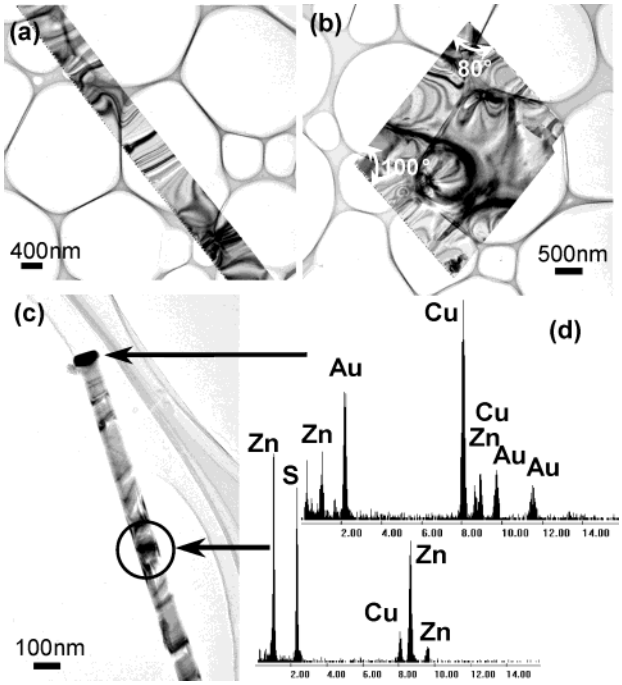

Figure 6. (a) TEM images of single ZnS nanobelts with saw-like edges, (b) ZnS nanosheet, and (c) ZnS nanorod attached to Au particles. (d) EDS spectra recorded from the stem part of the rod and from a particle at the end with dark contrast.

facets could be indexed from the crystallographic characteristics of the wurtzite ZnS as {0001} and {03-31}. The angle calculated between (0001) and (03-31) plane was either 80° or 100° (Figure 5c). In addition, small amounts of ZnS nanorods were detected (Figure 6c). The EDS spectrum for the rod structures revealed a composition similar to that of the belts and sheets. The particles attached to the ends of the rods were mainly composed of elemental Au. This result was confirmed by EDS analysis (Figure 6d). Results of the TED and HRTEM analyses revealed that the ZnS nanorods typically grew in the [0001] preferred direction.

The above results demonstrate that Au catalysts are important for the growth initiation of ZnS nanostructures, based on the VLS mechanism.[21] Although the sublimation point of ZnS is about 1200 °C, ZnS powders can evaporate at a lower temperature (970 °C), as was demonstrated in this experiment. Furthermore, similar results have also been obtained by our parallel experiments conducted at a temperature range of 950−980 °C. The ZnS vapor is preferentially condensed on the Au-coated sapphire substrate. From our investigation, it is believed that the ZnS vapor could directly condense and grow into micro-sized cubic ZnS crystals at the initial stages. As the reaction proceeds, the ZnS vapor forms an alloy with the Au to form a low-melting point liquid droplet on the surface of the micro-crystals. When the concentration of Zn and S atoms in the droplet are greater than the saturation threshold, the ZnS compound precipitates in wurtzite structure from the solid−liquid interface with preferential growth orientation. The Au catalyst played a crucial role for the formation of ZnS not only with unique morphology, but also with a metastable wurtzite-2H structure at relatively lower temperature. From the thermodynamic point of view, it is not favorable for the formation of ZnS in wurtzite structure from a melting droplet at temperatures lower than 1020 °C. In addition, the density and morphology of the structures varied from the upper to the lower parts of the

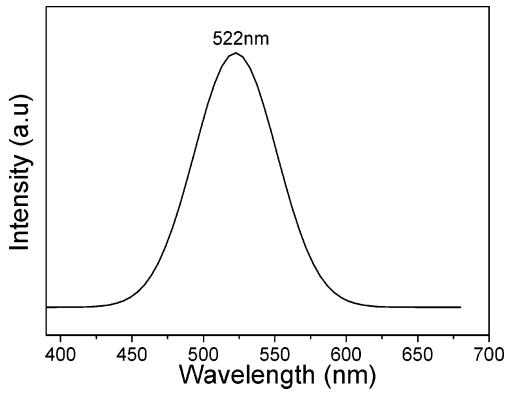

Figure 7. Room-temperature photoluminescence spectrum of ZnS nanobelts, showing a broad, strong green emission band centered at a wavelength of 522.5 nm.

tilted substrate. This was most likely caused by the growth kinetics such as the differences in local vapor pressure and temperature. However, there was no significant temperature gradient within the nanostructures-covered substrate. Thus, the difference of local vapor concentration may have played a crucial role on the morphology distribution of the formed nanostructures. Large nanosheets formed near the top due to higher vapor concentrations, whereas sparsely distributed nanostructures were observed in the lower part near the bottom of the ceramic boat because of insufficient vapor. Moreover, sheet-like, flag-like, bicrystal or tricrystal nanostructures were observed. Most of the attached Au particles were significantly smaller than the belt width. Some Au particles were also observed at the middle sites of nanostructures. These observations are difficult to explain in the context of VLS growth. Side epitaxial growth is known to have an important effect on the final morphology and structure of ZnS, related to the vapor−solid (VS) deposition process. If side epitaxial growth was dominant over the VLS growth, the attached particles could possibly be squeezed out, and finally stay at the middle sites or completely detach from the structures. Therefore, we would not find particles attached at the ends or other sites for some of the belts and sheets. The available evidence suggests that (1) the Au catalyst played a key role in the formation of wurtzite ZnS nanostructures, particularly at the initial stage of deposition. Under the conditions used in this study, if Au catalyst was not added, 1D nanostructures seldom formed. Only several pieces of large whisker-like material were sparsely deposited on the upper wall of the boat. However, using the Au-coated sapphire substrate, high-density belt-like products formed on the substrate and no obvious structures were deposited at other sites. (2) In the following stage, we propose that VS process also plays an important role particularly in the formation of nanosheets, flag-like, bicrystal and tricrystal nanobelts.

Figure 7 depicts the room-temperature photoluminescence (PL) spectrum recorded with a laser beam focused on the ZnS nanobelt. The PL spectrum revealed a strong and stable green emission band centered at 522.5 nm. When the laser beam was focused on an area with a high density of ZnS nanosheets, the PL spectrum showed a similar emission band, with only a slight decrease of intensity. No band gap emission from the ZnS was detected. Nanocrystalline ZnS doped with Cu^{2+}, Mn^{2+}, or rare earth ions is known to exhibit emissions with various visible colors due to different doping levels.[22] The strong green emission observed in this study was comparable to that of Cu^{2+}-doped ZnS nanocrystals.[23] In our experiments, except for the presence of Au, there was no other discernible impurities detected by EDX. The ZnS powder was also of high purity. Therefore it is likely that the strong green emission may have been related to the Au impurity-induced deep-level emission, similar to the PL characteristics of ZnS nanobelts and wires that have previously been reported. The green emission may also have been related to structural defects such as point defects that could potentially induce deep-level emission. Mitsui et al.[24] reported green emission (527 nm) from ZnS films induced by point defects generated by Ar ion milling. More systematic investigations are required to understand the origins of this PL emission band.

4. Conclusions

In summary, we demonstrated the formation of wurtzite ZnS nanostructures in the presence of Au catalysts using a simple thermal evaporation method at a temperature of 970 °C. The single crystalline ZnS belts ranged from tens to hundreds of micrometers in length and hundreds of nanometers in width and grew preferably in the [0001] or [01-11] direction. Large-sized nanosheets were found to be single crystalline with regular shapes and flat surfaces. ZnS nanorods were always observed growing along the [0001] direction with uniform diameter. The ends of the nanorods were attached to the Au particles, indicating that the conventional VLS process controlled the growth. However, the morphology and structure such as the large ZnS nanosheets, flag-like, bicrystal or tricrystal belts resulted from the combined effects of VS and VLS growth. Strong green emission of the ZnS nanobelts and nanosheets was also observed, and possibly explained with Au impurity and high density of defects. The ZnS nanostructures observed in this study could potentially be used in functionalized nanodevices. The technique used in this study is an effective approach for the large-scale formation of ZnS belts.

Acknowledgment. This work was supported by the Japan Society for the Promotion of Science (JSPS) Fellowship program at the National Institute of Advanced Industrial Science and Technology, Tsukuba, Japan.

References and Notes

(1) Huang, M. H.; Mao, S.; Feick, H.; Yan, H. Q.; Wu. Y. Y.; Kind, H.; Weber, E.; Russo, R.; Yang, P. D. *Science* **2001**, *292*, 1897.

(2) (a) Law, M.; Kind, H.; Messer, B.; Kim, F.; Yang. P. D. *Angew. Chem., Int. Ed. Engl.* **2002**, *41*, 2405. (b) Li, C.; Zhang, D. H.; Liu, X. L.; Han, S.; Tang, T.; Han, J.; Zhou, C. W. *Appl. Phys. Lett.* **2003**, *82*, 1613.

(3) Arnold, M. S.; Avouris, P.; Pan, Z. W.; Wang, Z. L. *J. Phys. Chem. B* **2003**, *107*, 659.

(4) Hughes, W. L.; Wang. Z. L. *Appl. Phys. Lett.* **2003**, *82*, 2886.

(5) (a) Liveri, V. T.; Rossi, M.; Arrigo, G. D.; Manno, D.; Micocci, G. *Appl. Phys. A.* **1999**, *69*, 369. (b) Murray, C. B.; Norris, D. J.; Bawendi, M. G. *J. Am. Chem. Soc.* **1993**, *115*, 8706.

(6) (a) Falcony, C.; Garcia, M.; Ortiz, A.; Alonso, J. C. *J. Appl. Phys.* **1992**, *72*, 1525. (b) Murase, N.; Jagannathan, R.; Kanematsu, Y.; Watanabe, M.; Kurita, A.; Hirata, K.; Yazawa, T.; Kushida, T. *J. Phys. Chem. B* **1999**, *103*, 754.

(7) Yamada, Y.; Yamamoto, S.; Nakamura, S.; Taguchi, T.; Sasaki, F.; Kobayashi, S.; Tani, T. *Appl. Phys. Lett.* **1996**, *69*, 88.

(8) Chen, W.; Wang, Z. G.; Lin, Z. J.; Lin, L. Y. *Appl. Phys. Lett.* **1997**, *70*, 1465.

(9) Agyeman, O.; Xu, C. N.; Suzuki, M.; Zheng, X. G. *J. Mater. Res.* **2002**, *17*, 959.

(10) Li, Y.; Wan, J. H.; Gu, Z. N. *Mol. Cryst. Liq. Cryst.* **1999**, *337*, 193.

(11) Wu, Q. S.; Zheng, N. W.; Ding, Y. P.; Li, Y. D. *Inorg. Chem. Commun.* **2002**, *5*, 671.

(12) Wang, Y. W.; Zhang, L. D.; Liang, C. H.; Wang, G. Z.; Peng, X. S. *Chem. Phys. Lett.* **2002**, *357*, 314.

(13) Li, Q.; Wang, C. R. *Appl. Phys. Lett.* **2003**, *83*, 359.

(14) Zhu, Y. C.; Bando, Y.; Xue, D. F. *Appl. Phys. Lett.* **2003**, *82*, 1769.

(15) Jiang, Y.; Meng, X. M.; Liu, J.; Xie, Z. Y.; Lee, C. S.; Lee, S. T. *Adv. Mater.* **2003**, *15*, 223.
(16) Ma, C.; Moore, D.; Li, J.; Wang, Z. L. *Adv. Mater.* **2003**, *15*, 228.
(17) Verma, A. R.; Krishma, P. *Polymorphism and Polytypism in Crystals;* Wiley: New York 1966.
(18) (a) Pan, Z. W.; Dai, Z. R.; Wang, Z. L. *Science* **2001**, *291*, 1947. (b) Dai, Z. R.; Pan, Z. W.; Wang Z. L. *J. Phys. Chem. B* **2002**, *106*, 902.
(19) Hirsch, P. B.; Howie, A.; Nicholson, R. B.; Pashley, D. W.; Whelan, M. J. *Electron Microscopy of Thin Crystals;* Butterworths: Markham, ON, Canada, 1965.
(20) Meng, X. M.; Jiang, Y.; Liu, J.; Lee, C.-S.; Bello, I.; Lee, S.-T. *Appl. Phys. Lett.* **2003**, *83*, 2244.
(21) Wagner, R. S.; Ellis, W. C. *Appl. Phys. Lett.* **1964**, *4*, 89.
(22) (a) Bhargava, R. N.; Gaillagher, D.; Hong, X.; Nurmikko, A. *Phys. Rev. Lett.* **1994**, *72*, 416. (b) Bol, A. A.; Meijerink, A. *J. Phys. Chem. B* **2001**, *105*, 10197. (c) Bol, A. A.; Meijerink, A. *J. Phys. Chem. B* **2001**, *105*, 10203. (d) Yu, I.; Senna, M. *Appl. Phys. Lett.* **1995**, *66*, 424. (e) Wang, M.; Sun, L.; Fu, X.; Liao, C.; Yan, C. *Solid State Commun.* **2000**, *115*, 493.
(23) Yang, P.; Lu, M. K.; Xu, D.; Yuan, D. L.; Zhou, G. J. *Chem. Phys. Lett.* **2001**, *336*, 76.
(24) (a) Mitsui, T.; Yamamoto, N.; Tadokoro, T.; Ohta, S. *J. Appl. Phys.* **1996**, *80*, 6972. (b) Mitsui, T.; Yamamoto, N. *Jpn. J. Appl. Phys.* **1998**, *37*, L1390.